The Astrophysical Journal Letters, 987:L36 (7pp), 2025 July 10 https://doi.org/10.3847/2041-8213/ade874


# New Clues on the Extended He II Ionization in IZw18 from GTC/MEGARA and JWST/MIRI

A. Arroyo-Polonio[1], C. Kehrig[1,2], J. M. Vílchez[1], J. Iglesias-Páramo[1,3], E. Pérez-Montero[1], S. Duarte Puertas[1,4], J. Gallego[5], and D. Reverte[6]
[1] Instituto de Astrofísica de Andalucía, CSIC, Apartado de correos 3004, 18080 Granada, Spain; aarroyo@iaa.es
[2] Observatório Nacional/MCTI, R. Gen. José Cristino 77, 20921-400 Rio de Janeiro, Brazil
[3] Centro Astronómico Hispano en Andalucía, Observatorio de Calar Alto, Sierra de los Filabres, 04550 Gérgal, Spain
[4] Departamento de Física Teórica y del Cosmos, Universidad de Granada, Granada, Spain
[5] Departamento de Física de la Tierra y Astrofísica, Universidad Complutense de Madrid, Spain
[6] Instituto de Astrofísica de Canarias, C/ Vía Láctea s/n, La Laguna, Tenerife, Spain
*Received 2025 April 30; revised 2025 June 25; accepted 2025 June 25; published 2025 July 8*

## Abstract

IZw18 is one of the lowest-metallicity star-forming galaxies known at $z \sim 0$, considered a unique local analogue of the first galaxies. The origin of its hard ionizing continuum, expected to be a common feature in the early Universe and traced by He II emission lines, remains intensely debated and challenging to explain. Here we combine optical Gran Telescopio Canarias MEGARA and mid-infrared (JWST/MIRI) integral field spectroscopic observations for IZw18 to shed new light on the high-ionization phenomenon. This Letter reports the first detection of the high-ionization [Ne V]14.32 $\mu$m line in IZw18. Its emission is spatially extended and coincident with the He II peak, revealing the presence of highly energetic ionizing sources that surpass mechanisms previously proposed on the basis of He II alone. Our kinematic studies highlight that the He II$\lambda$4686-emitting gas displays higher velocity dispersions and a different velocity pattern compared with the H$\beta$ emission, suggesting the presence of energetic processes such as shocks or stellar-driven feedback. Additionally, integrated spectra show asymmetric blueshifted profiles in the He II$\lambda$4686 line, possibly indicating early-stage stellar-driven outflows potentially facilitating future ionizing photon leakage. Our spatial analysis also reveals differences in structure between the emission of H$\beta$ and He II$\lambda$4686, with the He II$\lambda$4686 peak offset by a projected distance of 140 pc from the peak H$\beta$ emission. This indicates distinct locations for the most extreme ionizing sources compared to moderate ionizing sources. Our findings underscore the complex interplay of physical processes in extremely metal-poor environments with highly ionized gas, offering new insights into the conditions prevailing in the early galaxies.

*Unified Astronomy Thesaurus concepts:* Galaxies (573); Blue compact dwarf galaxies (165); Starburst galaxies (1570); Interstellar medium (847); Stellar feedback (1602); Metallicity (1031); Ionization (2068); Photoionization (2060); H II regions (694); Galaxy physics (612); Galaxy kinematics (602); Emission line galaxies (459)

## 1. Introduction

The detection of nebular (narrow) He II recombination lines, particularly at $\lambda$1640 Å (UV) and $\lambda$4686 Å (optical), in star-forming (SF) galaxies signals the presence of hard radiation (Energy $\geqslant$ 4 Ry $\sim$ 54.4 eV). The nature and origin of such high-ionization lines, especially in metal-poor SF systems, remains unexplainable and is actively debated in the literature (e.g., D. R. Garnett et al. 1991; C. Kehrig et al. 2015; L. M. Oskinova & D. Schaerer 2022). This persistent ambiguity about the sources capable of doubly ionizing helium hampers our interpretation of the nebular He II emission lines in high-redshift galaxies and, by extension, our understanding of the epoch of reionization. Different mechanisms have been proposed to explain this phenomenon, including hot Wolf–Rayet stars (e.g., D. R. Garnett et al. 1991; C. Kehrig et al. 2011; M. Shirazi & J. Brinchmann 2012; A. Roy et al. 2025), shocks (e.g., A. Plat et al. 2019; L. M. Oskinova & D. Schaerer 2022), X-ray sources (e.g., P. Senchyna et al. 2020; C. Kehrig et al. 2021; C. Simmonds et al. 2021), and peculiar (nearly) metal-free hot stars, or Pop III–like stars (e.g., D. Schaerer 2002; P. Cassata et al. 2013; C. Kehrig et al. 2015, 2018; T. Nanayakkara et al. 2019; E. Pérez-Montero et al. 2020; A. Venditti et al. 2024).

Observations indicate an anticorrelation of the He II line intensity with metallicity (e.g., N. G. Guseva et al. 2000; M. Shirazi & J. Brinchmann 2012), while He II-emitters are expected to be more frequent in the high-$z$ Universe (e.g., D. Schaerer 2002; E. R. Stanway & J. Eldridge 2019). This trend aligns with theoretical predictions indicating that lower-metallicity galaxies exhibit harder ionizing spectral energy distributions (SEDs), more frequent in early-Universe conditions (e.g., R. Smit et al. 2015; E. R. Stanway & J. Eldridge 2019). Recent rest-frame-UV surveys have indeed uncovered dozens of strong He II$\lambda$1640 emitters at $2 \lesssim z \lesssim 6$ (e.g., P. Cassata et al. 2013; T. Nanayakkara et al. 2019; A. Saxena et al. 2020). Yet, despite deep observations, the large distances preclude spatially resolved studies and hinder multiwavelength diagnostics, so the detailed physical conditions in these high-$z$ systems remain poorly constrained.

Local analogs of high-$z$ ($z \gtrsim 2$) SF galaxies (including those that dominated the epoch of reionization ($z \gtrsim 6$)) provide crucial laboratories for studying the properties of highly ionized gas thanks to their higher apparent magnitudes and spatial resolution. The SF dwarf galaxy IZw18 is a remarkable

analog, not only for high-$z$ SF galaxies in general, but for a particular subset of these galaxies that present He II emission, a feature frequently seen in LyC leakers (e.g., E. Vanzella et al. 2020; R. P. Naidu et al. 2022; D. Schaerer et al. 2022; A. U. Enders et al. 2023; C. Mondal et al. 2025). This is because of its extremely low metallicity (12 + log (O/H) = 7.11, ∼3% solar; e.g., J. M. Vílchez & J. Iglesias-Pá 1998; C. Kehrig et al. 2016) and also due to its highly extended nebular He II-emitting region (∼5" diameter ∼400 pc at the distance of 18.2 Mpc; A. Aloisi et al. 2007), which is spatially coincident with the northwest SF knot, and with a corresponding very high He II luminosity ($1.12 \pm 0.07 \times 10^{38}$ erg s$^{-1}$). These features were unveiled for the first time, based on integral field spectroscopic (IFS) data, in C. Kehrig et al. (2015), who find that the observed He II ionization budget of IZw18 can be explained by peculiar hot (nearly) metal-free massive stars (see also C. Kehrig et al. 2018). In C. Kehrig et al. (2021), the authors discard X-ray photons as the dominant He II ionizing mechanism in IZw18, highlighting the complex nature of He II emission in this galaxy, which keeps challenging state-of-the-art models (e.g., E. R. Stanway & J. Eldridge 2019; J. J. Eldridge & E. R. Stanway 2022). Additionally, R. J. R. Vaught et al. (2021) revealed notable velocity offsets (∼30 km s$^{-1}$) between the He II-emitting gas and the bulk of the ionized gas traced by Balmer lines in IZw18 (see also A. Arroyo-Polonio et al. 2024), suggesting dynamic decoupling and adding complexity to our understanding of the He II ionization problem.

Regarding the presence of other high-ionization lines in IZw18, X-ray observations marginally revealed the extremely high-ionization line O VIII in IZw18 (D. Bomans & K. Weis 2002; T. X. Thuan et al. 2004), which indicates the presence of photons with energies above 59 Ry. Nevertheless, T. X. Thuan & Y. I. Izotov (2005) searched for the high-ionization [Ne V]$\lambda$3426 emission line (ionization potential (IP) of 97.1 eV) in several SF dwarfs and did not detect such a line in IZw18 (see also Y. Izotov et al. 2021).

Additionally, H. Atek et al. (2009) identified pronounced Ly$\alpha$ absorption in the northwest region of IZw18, close to the He II$\lambda$4686 emission. Their radiative transfer models pointed to a high neutral hydrogen column density ($N_{\rm H\,I} \simeq 6.5 \times 10^{21}$ cm$^{-2}$) significantly suppressing the escape of Ly$\alpha$ and LyC photons into the intergalactic medium, even in conditions of minimal dust. Complementing this, several studies (e.g., R. Maiolino et al. 2017; S. R. Flury et al. 2023, 2025; A. Arroyo-Polonio et al. 2024; C. A. Carr et al. 2025) emphasize the critical role of energetic outflows in shaping nebular-line profiles, often manifesting as broad, blueshifted wings. Such outflows can carve low-density pathways facilitating LyC photon escape, highlighting that stellar-driven outflows play a vital role in photon leakage processes (e.g., R. Amorín et al. 2024).

In this Letter, we take advantage of new optical Gran Telescopio Canarias (GTC) MEGARA (A. G. Gil de Paz et al. 2016) and mid-infrared (James Webb Space Telescope (JWST)/MIRI) IFS data to shed new light on the puzzling source(s) of the high-energy ionizing continuum (>54 eV) in IZw18.

## 2. Observations

This Letter combines GTC/MEGARA optical IFS observations with archival mid-infrared IFS data from JWST/MIRI, complemented by archival imaging data from JWST/NIRCam and the Hubble Space Telescope (HST).

Optical observations of IZw18 were conducted on 2022 February 6 using the MEGARA instrument (LR-B grating; $R \sim 6000$) at the GTC, located at the Roque de los Muchachos Observatory (Spain). The Integral Field Unit (IFU) of MEGARA provides a field of view of $12.5 \times 11.3$ arcsec$^2$, composed of 567 hexagonal spaxels (0.″62 per spaxel), covering a spectral range of approximately ∼4330–5200 Å. Three exposures of 1200 s were obtained on 2022 February 6, with a measured seeing of 1″ during the observations, targeting the entire main body (MB) of IZw18 (R.A. = 09:34:01.98, decl. = 55:14:26.5, J2000.0). The data reduction was performed following the procedure described in A. Arroyo-Polonio et al. (2024). The resulting data enable the generation of detailed maps of the structure and kinematics, particularly of the He II$\lambda$4686 and H$\beta$ emission lines.

Moreover, we used archival mid-infrared IFU data from the MIRI Medium Resolution Spectrometer (MRS) of the JWST. These observations targeted the northwest knot of IZw18 and were conducted between 2024 March 8 and 9, as part of JWST Cycle 2 (PI: A. Aloisi, program 03533). We used all three MRS grating settings (SHORT, MEDIUM, LONG) within channel 3, covering wavelengths from ∼11.5 to 18 $\mu$m. This channel has a field of view of $5.2 \times 5.5$ arcsec$^2$, with a spectral resolving power ranging approximately from $R \sim 3000$ at 12 $\mu$m to $R \sim 2000$ at 18 $\mu$m. The spatial resolution is diffraction-limited, varying from ∼0.″4 at the shortest wavelengths to ∼0.″6 at the longest wavelengths. The full MIRIFULONG detector array operated in SLOWR1 readout mode with a four-point dither pattern optimized for extended emission, achieving a total integration time of ∼29,146 s. The retrieved data are Level 3 science-ready calibrated products. The combination of these optical and mid-infrared IFS observations carried out in this work allowed us to analyze the galaxy structure and ionization covering from 1 Ry to high-ionization lines such as [Ne V] 14.32 $\mu$m (IP of ∼7.1 Ry).

Additionally, we make use of archival imaging observations from JWST/NIRCam obtained with the F115W filter (PI: M. Margaret, $\lambda_c \sim 1.15\,\mu$m), as well as HST data acquired with Advanced Camera for Surveys Wide Field Channel (WFC) using the F606W filter (PI: A. Aloisi, $\lambda_c \sim 0.606\,\mu$m) and WFC3/UVIS with the F225W filter (PI: G. Oestlin, $\lambda_c \sim 0.225\,\mu$m).

Some of the data presented in this Letter were obtained from the Mikulski Archive for Space Telescopes at the Space Telescope Science Institute. The specific observations analyzed can be accessed via DOI: 10.17909/yjfs-gc89.

## 3. Data Analysis

### 3.1. Optical GTC/MEGARA IFS

We investigated the spatial distribution, structure, and kinematics of the ionized gas in the MB of IZw18 by analyzing two emission lines: H$\beta$ and He II$\lambda$4686. These lines, each requiring different IPs (13.6 eV for H$\beta$ and 54.4 eV for He II$\lambda$4686), allowed us to sample the ionization structure within the ionized region. H$\beta$ maps the H II region and He II$\lambda$4686 isolates an extended highly ionized zone (the He III region). By comparing these differently ionized layers, we gain a clearer, ionization-dependent view of the ionized gas in the galaxy.

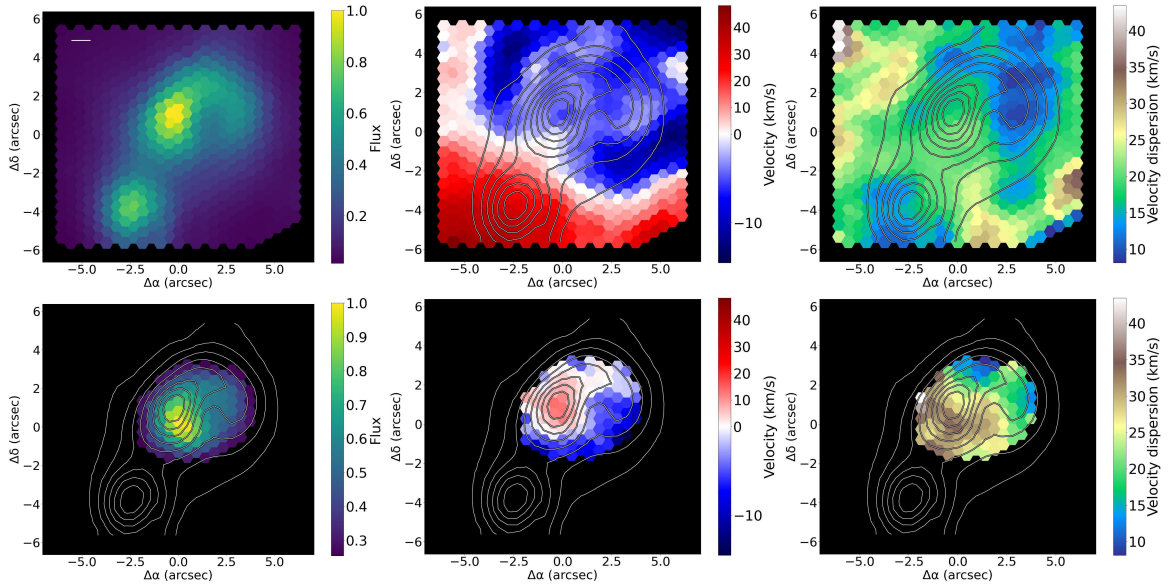


**Figure 1.** Maps of the flux (left), radial velocity (middle), and radial velocity dispersion (right) of the selected emission lines: H$\beta$ (top) and He II$\lambda$4686 (bottom). The isocontours overplotted in all panels (except for the top-left one) represent the H$\beta$ flux for reference. The white bar shown in the top-left panel represents 1″ (i.e., ∼88 pc), which is the FWHM of the Gaussian kernel used to smooth the data. Black spaxels represent those that do not follow our criterion (S/N > 3 and $\sigma > \sigma_{\rm ins}$). In all figures in the Letter, north is up and east is to the left.

For each spaxel within the GTC/MEGARA data cube, we fit single Gaussians to the emission lines to measure line flux, velocity, and velocity dispersion, following the relativistic Doppler formula and velocity dispersion correction described in A. Arroyo-Polonio et al. (2024), which subtracts the instrumental and thermal broadening ($\sigma_{\rm inst}$ and $\sigma_{\rm thermal}$) from the observed width so that $\sigma^2 = \sigma^2_{\rm obs} - (\sigma^2_{\rm inst} + \sigma^2_{\rm thermal})$. A Gaussian smoothing kernel of FWHM = 1″ (see top-left panel in Figure 1) is applied to enhance the signal-to-noise ratio (S/N) and coherence between spaxels (A. Arroyo-Polonio et al. 2024). We excluded spaxels if their emission-line FWHM was below the instrumental FWHM ($\sigma_{\rm inst} = 0.45$ Å) or if the S/N fell below 3. Finally, all velocities are reported relative to the systemic velocity determined from the integrated H$\beta$ profile of the entire galaxy.

The maps of H$\beta$ and He II$\lambda$4686 (see Figure 1) reveal notable differences in the morphology and kinematics of the ionized gas in the MB of IZw18.

The He II$\lambda$4686 flux map shows an extended emission across the northwest knot similar to the one seen in H$\beta$ (left panels in Figure 1), but the peaks of the two emission lines are displaced 1.″6 (140 pc projected at the distance of 18.2 Mpc; see also C. Kehrig et al. 2015). This offset implies that the bulk of the ionizing sources producing photons with energies >1 Ry (traced by H$\beta$) does not coincide spatially with the harder subsample of sources responsible for photons of >4 Ry (traced by He II$\lambda$4686). The gas structure of the He III region is not necessarily the same as that of the overall HII region. Consequently, the brightest sources in the H II region (as traced by H I recombination lines) does not necessarily trace the hard radiation fields. Furthermore, this spatial offset might suggest a scenario of star formation propagation; however, given the still unclear nature of the He II ionizing sources, such interpretation remains somewhat speculative. In addition, the velocity structure (middle panels in Figure 1) in the He II$\lambda$4686 region does not match the overall rotational pattern as H$\beta$ does. Furthermore, at the position of the H$\beta$ peak, the He II$\lambda$4686 emission line is redshifted by $\sim$+20 km s$^{-1}$ compared to the velocity of the H$\beta$ gas (similar results are found in R. J. R. Vaught et al. 2021). This redshift might indicate that the He II$\lambda$4686-emitting gas is situated deeper along the line of sight and/or is significantly influenced by localized feedback mechanisms. Regarding the velocity dispersion maps (right panels in Figure 1), the He II$\lambda$4686 line shows significantly higher velocity dispersions, being above 25 km s$^{-1}$ in a great portion of the region (meanwhile, H$\beta$ is below 25 km s$^{-1}$ in the He II-emitting region) and exceeding 40 km s$^{-1}$ in certain areas. This broader linewidth suggests that the He II$\lambda$4686-emitting gas experiences additional kinetic energy input. The physical processes behind this could be shocks, intense stellar feedback, or enhanced turbulence in highly energetic environments (e.g., R. L. Davies et al. 2017; D. S. Rupke 2018; X. Yu et al. 2019).

We also extracted an integrated spectrum by adding the emission from all He II-emitting spaxels with S/N > 3 in the He II flux (see bottom-left panel in Figure 1) with the aim to perform a detailed analysis of the line profiles shown in Figure 2.

For the line profiles of both He II$\lambda$4686 and H$\beta$, a Gaussian fit is made along with the velocity of the center of mass ($v_{\rm CM}$), retrieved by using the equation

$$v_{\rm CM} = \frac{\sum_i F_i \times v_i}{\sum_i F_i},$$

where $F_i$ is the flux in each spectral pixel and $v_i$ is the velocity corresponding to the same spectral pixel. The $v_{\rm CM}$ provides a mass-weighted average velocity of the emitting gas, offering a physically motivated estimate of the motion of each ionized region (H II and He III regions). It is particularly useful in cases where the line is asymmetric or shows broadening due to outflows, as it reflects the net kinematic behavior of the gas. The range of integration in order to retrieve the $v_{\rm CM}$ is taken from −165 to 165 km s$^{-1}$ (4 times the FWHM of the He II$\lambda$4686 line profile). This choice ensures that the vast majority of the line

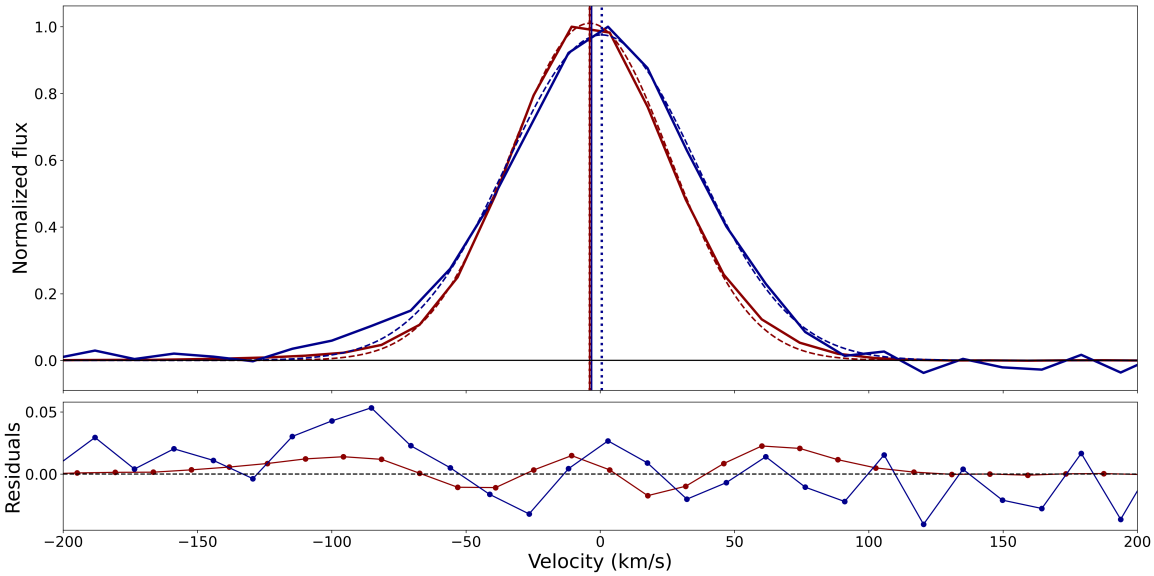


**Figure 2.** Line profiles of H$\beta$ (in red) and He II$\lambda$4686 (in blue). In the upper part, solid lines represent the observed line profiles and dashed lines the best Gaussian fit of each line. Vertical dotted lines represent the centroid of each Gaussian. Vertical solid lines represent the centers of mass of each profile. In the bottom part, the residuals (observation—Gaussian fit) are represented. The flux of each line is normalized to its peak value.

emission, including possible extended wings due to turbulent or outflowing gas, is included in the computation while minimizing the contribution from noise-dominated continuum regions. To quantify the uncertainties associated with all these measurements, we employed the bootstrapping method (B. Efron & R. Tibshirani 1985; see Table 1).

In agreement with the spatially resolved results, the line profiles clearly show that H$\beta$ has a lower velocity dispersion in comparison to He II$\lambda$4686. Furthermore, the He II$\lambda$4686 peak is redshifted in comparison with the H$\beta$ peak.

Beyond simply corroborating the earlier findings (higher velocity dispersion and redshifted peak in the He II$\lambda$4686 line relative to H$\beta$), the integrated spectrum reveals a new feature in the He II$\lambda$4686 line profile, a subtle blue-wing extension (bluer than $-100\,\mathrm{km\,s^{-1}}$) not clearly discernible in the spatial maps. This asymmetric line shape may indicate the presence of a blueshifted outflow (e.g., R. Amorín et al. 2024) in the highly ionized He II$\lambda$4686 region. To quantify this asymmetry we can compare the Gaussian centroid with $v_{\rm CM}$. The higher the difference between these two, the greater the asymmetry in the profile. As shown in Table 1, the Gaussian centroid of H$\beta$ nearly coincides with its $v_{\rm CM}$, both registering around $4\,\mathrm{km\,s^{-1}}$. In contrast, while the He II$\lambda$4686 $v_{\rm CM}$ remains close to $4\,\mathrm{km\,s^{-1}}$, its Gaussian centroid is approximately $0\,\mathrm{km\,s^{-1}}$.

The fact that the H$\beta$ and He II$\lambda$4686 regions share the $v_{\rm CM}$, together with the asymmetry in the He II$\lambda$4686 profile (characterized by a blue wing and a redshifted peak), opens up the possibility of an off-centered feedback mechanism in the He III region, which is pushing a small fraction of gas with high velocity toward the blue. The conservation of momentum thus requires the other bigger fraction of He III gas to move toward the red, as seen in the redshift peak. This may indicate an early-stage outflow (some related studies investigating the inner outflow region and ionization dependency of the outflow are M. S. Westmoquette et al. 2007; J. Chisholm et al. 2016) that, depending on its kinetic energy and the mass it will encounter through its way out, could carve a path for ionizing photons that may eventually escape. We estimated the mechanical energy injected into the He III region by adopting a radius of $R = 200\,\mathrm{pc}$ (i.e., a 400 pc diameter), a mean electron density of $n_{\rm e} = 100\,\mathrm{cm^{-3}}$, a volume filling factor of $f = 0.1$, and an observed velocity dispersion of $\sigma = 30\,\mathrm{km\,s^{-1}}$ (Table 1). Under these conditions, the kinetic energy is

$$E_{\rm kin} = \frac{3}{2} M\,\sigma^2,\ M = (\mu\, m_{\rm H}\, n_{\rm e})\left(\frac{4}{3}\pi R^3\right) f,$$

where $\mu \simeq 1.4$ is the mean molecular weight of primordial H/He gas and $m_{\rm H}$ is the proton mass. Substituting the above values yields $E_{\rm kin} \simeq 3 \times 10^{53}$ erg, an order of magnitude result consistent with STARBURST99 for a $10^6\,M_\odot$ young star cluster (C. Leitherer et al. 1999). This mass compares well with the stellar mass of the northwest knot (e.g., F. Annibali et al. 2013), suggesting that feedback from this knot could comfortably power the observed dispersion in velocity. Nevertheless, recent observations indicate that IZw18 exhibits significant opacity to both LyC and Ly$\alpha$ photons (H. Atek et al. 2009).

**Table 1**
Kinematic Properties of the Emission Lines in the Integrated Spectrum

| Emission Line | Velocity ($\mathrm{km\,s^{-1}}$) | Velocity Dispersion ($\sigma$) ($\mathrm{km\,s^{-1}}$) | $v_{\rm CM}$ ($\mathrm{km\,s^{-1}}$) |
|---|---|---|---|
| (1) | (2) | (3) | (4) |
| H$\beta$ | $-3.91 \pm 0.04$ | $16.07 \pm 0.07$ | $-3.9 \pm 0.2$ |
| He II$\lambda$4686 | $0.6 \pm 0.3$ | $27.0 \pm 0.6$ | $-4 \pm 2$ |

**Note.** Column (1): analyzed emission line. Column (2): radial velocity. Column (3): radial velocity dispersion. Column (4): radial velocity of the center of mass.

### 3.2. Mid-infrared JWST/MIRI IFS

Until now, [Ne V] emission have never been observed in the galaxy IZw18. In this work, using IFS observations from JWST/MIRI, we report the detection of the [Ne V]14.32 $\mu$m

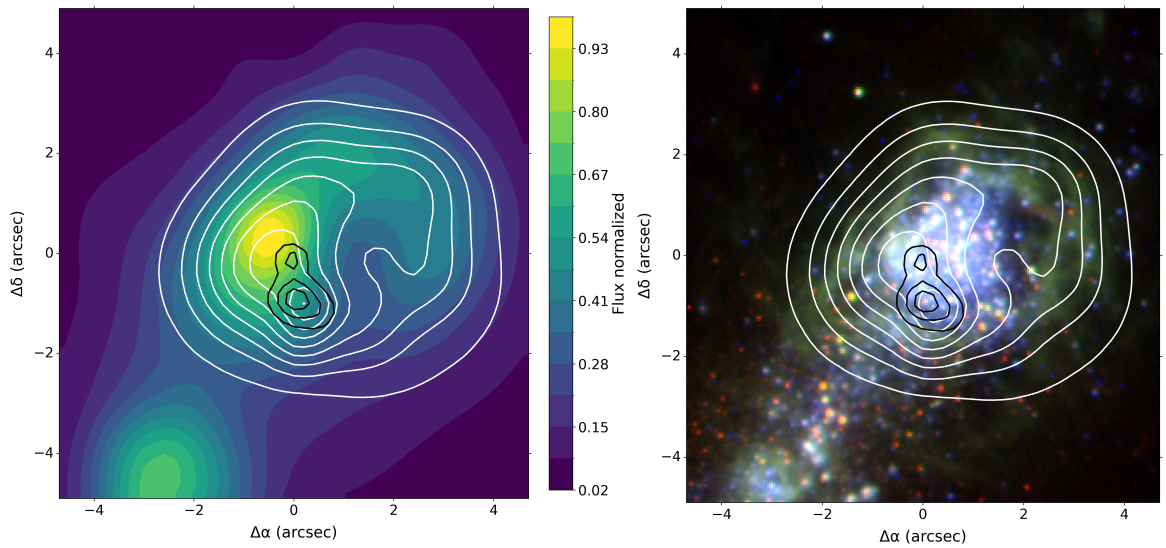


**Figure 3.** (Left panel) The MEGARA H$\beta$ emission map as a color-filled contour plot, smoothed using bilinear interpolation. For reference, the isocontours of the MEGARA He II$\lambda$4686 and the MIRI [Ne V]14.32 $\mu$m emissions are overplotted in white and black, respectively. (Right panel) Color-composite image in three bandpasses: near-infrared JWST NIRCam/F115W continuum at $\sim$1.15 $\mu$m (red), optical HST Advanced Camera for Surveys F606W continuum at $\sim$6060 Å (green), and HST WFC3/UVIS/F225W at $\sim$2250 Å (blue); the same isocontours of He II$\lambda$4686 and [Ne V]14.32 $\mu$m line emissions are displayed.

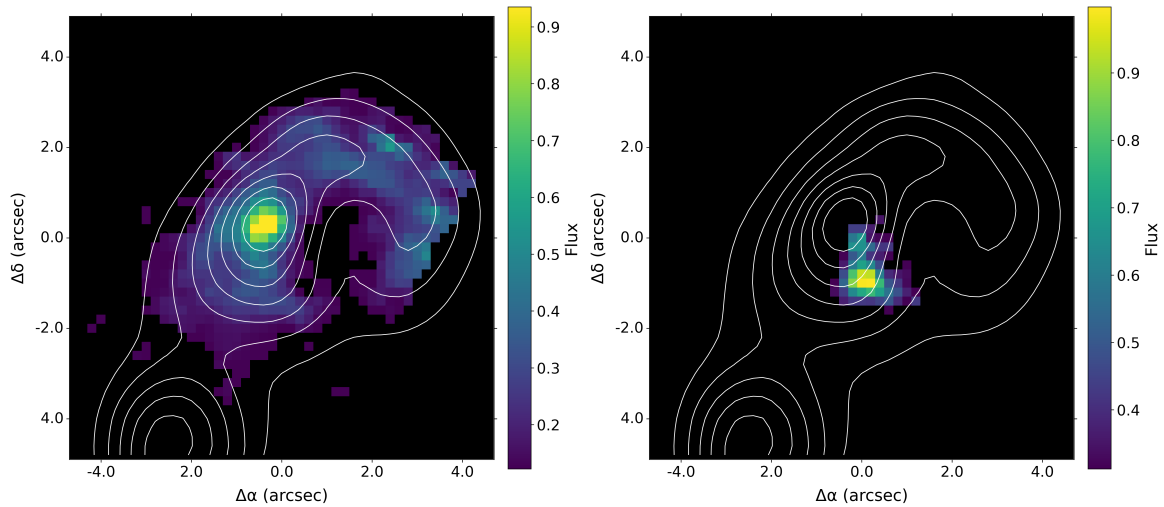


**Figure 4.** (Left panel) The MIRI Hu$\alpha$ emission map. For reference, the isocontours of the MEGARA H$\beta$ emission are overplotted in white. (Right panel) The MIRI [Ne V]14.32 $\mu$m emission map. Again, for reference, the isocontours of the MEGARA H$\beta$ emission are overplotted in white.

line in IZw18 for the first time. This emission originates from an ion with IP of 97.1 eV, nearly twice as high as that of He II$\lambda$4686 (see Figure 3 and the right panel in Figure 4).

Previous attempts to detect [Ne V] emission in IZw18 (T. X. Thuan & Y. I. Izotov 2005 searching for the [Ne V] 3426 Å line) were unsuccessful, likely due to observational limitations. Our detection benefits from the superior spatial and spectral resolution of JWST/MIRI (approximately 0.″5 and $R \sim 2400$ at 14.3 $\mu$m). Additionally, for the electron temperature and density of IZw18 ($T_e \sim 20{,}000$ K, $n_e < 300\,\mathrm{cm}^{-3}$; e.g., C. Kehrig et al. 2016), the emissivity of the [Ne V] 14.32 $\mu$m line is roughly 70% higher than that of the [Ne V] 3426 Å line (atomic data: CHIANTI v11; R. Dufresne et al. 2024; computed with PYNEB V. Luridiana et al. 2015), significantly facilitating the detection of [Ne V] in the IR.

To spatially correlate the JWST/MIRI and GTC/MEGARA cubes, we proceeded by performing a careful spatial matching of the peak position of the H$\beta$ emission line from GTC/MEGARA with that of the Humphrey-$\alpha$ line observed with JWST/MIRI (see the right panel in Figure 4). This precise spatial correlation of the H peaks allowed us to find that the peak emission of the [Ne V]14.32 $\mu$m line coincides very closely with the peak of the He II$\lambda$4686 emission. Figure 3 also shows that the [Ne V] emitting region is extended [$\sim$1.″8] (corresponding to a projected distance of $\sim$160 pc), while covering a smaller area than that of the He II-emitting region within the northwest knot.

The nebular He II$\lambda$4686 ionization (IP of 4 Ry) in IZw18, still an open question, has been attributed to peculiar, nearly metal-free hot stars (Pop III–like stars; see C. Kehrig et al. 2015, 2021). This new detection of the extended [Ne V] emission (IP of 7.1 Ry) and the spatial coincidence between the He II$\lambda$4686 and [Ne V] emitting zones have important implications for better understanding the high-ionization

sources in IZw18. These results not only reinforce the existence of a very hard SED within the northwest knot (see how the [Ne V] emission overlaps with some resolved stellar sources; right panel of Figure 3) but also indicates the presence of much harder ionizing photons ($E > 97$ eV is needed to produce Ne V; e.g., M. Mingozzi et al. 2025), opening the possibility of additional ionization mechanisms, which will be studied in detail in a future work.

## 4. Conclusions

In this study, we conducted a detailed analysis of the ionized gas in the MB of IZw18 using the emission lines H$\beta$, He II$\lambda$4686, and [Ne V]14.32 $\mu$m (each one tracing ionized gas at different ionization stages: 13.6, 54.4, and 97.1 eV) using the IFS from GTC/MEGARA and JWST/MIRI. Our primary findings are summarized as follows:

1. The spatial distribution of H$\beta$ and He II$\lambda$4686 emission lines reveals differences in their structure, with the He II-emitting region peak offset by a projected distance of 140 pc from the peak H$\beta$ emission. This spatial separation indicates that the most extreme ionizing sources, responsible for the He II emission, are concentrated away from the bulk of lower-energy (13.6 eV) ionizing sources traced by H$\beta$.
2. The kinematic analysis shows that He II gas exhibits higher velocity dispersions and a different velocity pattern compared to that of the H$\beta$ emission. This indicates that the He II emission region is kinematically decoupled from the H II region, possibly due to energetic processes such as localized stellar feedback or shocks, indicative of highly turbulent environments.
3. Integrated spectral analysis reveals an asymmetric, blueshifted extension in the He II$\lambda$4686 profile, interpreted as evidence of early-stage stellar-driven outflow. Such outflow might potentially facilitate future ionizing photon leakage despite current observations of high Ly$\alpha$ opacity.
4. Using JWST/MIRI data, we report the first detection of the [Ne V]14.32 $\mu$m emission line in IZw18. The presence of [Ne V] extended emission indicates ionizing sources with energies significantly exceeding those previously inferred solely from He II emission. Additionally, the spatial coincidence between the peaks of [Ne V] and He II emissions suggests that the same highly energetic sources responsible for the [Ne V] emission likely contribute to the bulk of He II$\lambda$4686 emission.

Our results highlight the complexity and diversity of ionizing mechanisms at play within extremely metal-poor galaxies like IZw18, providing valuable insights into conditions analogous to those of early-Universe galaxies.

## Acknowledgments

A.A.P. acknowledges financial support from the State Agency for Research of the Spanish MCIU through the Center of Excellence Severo Ochoa' award to the Instituto de Astrofísica de Andalucía CEX2021- 001131-S funded by MCIN/AEI/10.13039/501100011033, and from the grant PID2022-136598NB-C32 "Estallidos8." A.A.P. acknowledges support from the project AST22_00001_Subp_11 funded by the EU—NextGenerationEU. The authors acknowledge the plan PID2021-123417OB-I00.

## ORCID iDs

A. Arroyo-Polonio https://orcid.org/0000-0002-9523-8016
C. Kehrig https://orcid.org/0000-0003-1231-1482
J. M. Vílchez https://orcid.org/0000-0001-7299-8373
J. Iglesias-Páramo https://orcid.org/0000-0003-2726-6370
E. Pérez-Montero https://orcid.org/0000-0003-3985-4882
S. Duarte Puertas https://orcid.org/0000-0002-5542-1940
J. Gallego https://orcid.org/0000-0003-1439-7697
D. Reverte https://orcid.org/0000-0003-0456-149X

## References

Aloisi, A., Clementini, G., Tosi, M., et al. 2007, ApJL, 667, L151
Amorín, R., Rodríguez-Henríquez, M., Fernández, V., et al. 2024, A&A, 682, L25
Annibali, F., Cignoni, M., Tosi, M., et al. 2013, AJ, 146, 144
Arroyo-Polonio, A., Kehrig, C., Paramo, J. I., et al. 2024, A&A, 687, A77
Atek, H., Schaerer, D., & Kunth, D. 2009, A&A, 502, 791
Bomans, D., & Weis, K. 2002, in ASP Conf. Ser. 262, The High Energy Universe at Sharp Focus: Chandra Science, ed. E. M. Schlegel & S. D. Vrtilek (San Francisco, CA: ASP), 141
Carr, C. A., Cen, R., Scarlata, C., et al. 2025, ApJ, 982, 137
Cassata, P., Le Fèvre, O., Charlot, S., et al. 2013, A&A, 556, A68
Chisholm, J., Tremonti, C. A., Leitherer, C., Chen, Y., & Wofford, A. 2016, MNRAS, 457, 3133
Davies, R. L., Groves, B., Kewley, L. J., et al. 2017, MNRAS, 470, 4974
Dufresne, R., Del Zanna, G., Young, P., et al. 2024, ApJ, 974, 71
Efron, B., & Tibshirani, R. 1985, Behaviormetrika, 12, 1
Eldridge, J. J., & Stanway, E. R. 2022, ARA&A, 60, 455
Enders, A. U., Bomans, D. J., & Wittje, A. 2023, A&A, 672, A11
Flury, S. R., Jaskot, A. E., Saldana-Lopez, A., et al. 2025, ApJ, 985, 128
Flury, S. R., Moran, E. C., & Eleazer, M. 2023, MNRAS, 525, 4231
Garnett, D. R., Kennicutt, R. C., Chu, Y.-H., & Skillman, E. D. 1991, PASP, 103, 850
Gil de Paz, A. G., Carrasco, E., Gallego, J., et al. 2016, Proc. SPIE, 9908, 99081K
Guseva, N. G., Izotov, Y. I., & Thuan, T. X. 2000, ApJ, 531, 776
Izotov, Y., Thuan, T., & Guseva, N. 2021, MNRAS, 508, 2556
Kehrig, C., Guerrero, M. A., Vílchez, J., & Ramos-Larios, G. 2021, ApJL, 908, L54
Kehrig, C., Oey, M., Crowther, P., et al. 2011, A&A, 526, A128
Kehrig, C., Vílchez, J., Guerrero, M. A., et al. 2018, MNRAS, 480, 1081
Kehrig, C., Vílchez, J., Pérez-Montero, E., et al. 2015, ApJL, 801, L28
Kehrig, C., Vílchez, J., Pérez-Montero, E., et al. 2016, MNRAS, 459, 2992
Leitherer, C., Schaerer, D., Goldader, J. D., et al. 1999, ApJS, 123, 3
Luridiana, V., Morisset, C., & Shaw, R. A. 2015, A&A, 573, A42
Maiolino, R., Russell, H., Fabian, A. C., et al. 2017, Natur, 544, 202
Mingozzi, M., Del Valle-Espinosa, M. G., James, B. L., et al. 2025, ApJ, 985, 253
Mondal, C., Saha, K., Borgohain, A., et al. 2025, arXiv:2506.06831
Naidu, R. P., Matthee, J., Oesch, P. A., et al. 2022, MNRAS, 510, 4582
Nanayakkara, T., Brinchmann, J., Boogaard, L., et al. 2019, A&A, 624, A89
Oskinova, L. M., & Schaerer, D. 2022, A&A, 661, A67
Pérez-Montero, E., Kehrig, C., Vílchez, J., et al. 2020, A&A, 643, A80
Plat, A., Charlot, S., Bruzual, G., et al. 2019, MNRAS, 490, 978
Roy, A., Krumholz, M., Salvadori, S., et al. 2025, A&A, 696, A29
Rupke, D. S. 2018, Galax, 6, 138
Saxena, A., Pentericci, L., Schaerer, D., et al. 2020, MNRAS, 496, 3796
Schaerer, D. 2002, A&A, 382, 28
Schaerer, D., Marques-Chaves, R., Barrufet, L., et al. 2022, A&A, 665, L4
Senchyna, P., Stark, D. P., Mirocha, J., et al. 2020, MNRAS, 494, 941
Shirazi, M., & Brinchmann, J. 2012, MNRAS, 421, 1043
Simmonds, C., Schaerer, D., & Verhamme, A. 2021, A&A, 656, A127
Smit, R., Bouwens, R. J., Franx, M., et al. 2015, ApJ, 801, 122
Stanway, E. R., & Eldridge, J. 2019, in IAU Symp. 352, Uncovering Early Galaxy Evolution in the ALMA and JWST Era (Cambridge: Cambridge Univ. Press), 84
Thuan, T. X., Bauer, F. E., Papaderos, P., & Izotov, Y. I. 2004, ApJ, 606, 213

Thuan, T. X., & Izotov, Y. I. 2005, ApJS, 161, 240
Vanzella, E., Caminha, G., Calura, F., et al. 2020, MNRAS, 491, 1093
Vaught, R. J. R., Sandstrom, K. M., & Hunt, L. K. 2021, ApJL, 911, L17
Venditti, A., Bromm, V., Finkelstein, S. L., et al. 2024, ApJL, 973, L12
Vílchez, J. M., & Iglesias-Pá, J. 1998, ApJ, 508, 248
Westmoquette, M. S., Smith, L. J., Gallagher, J. S., & Exter, K. M. 2007, MNRAS, 381, 913
Yu, X., Shi, Y., Chen, Y., et al. 2019, MNRAS, 486, 4463